Steady Swimming and Routine Maneuvering by Eels: A Baseline for Biomimetic Undulatory Propulsors

Eric D. Tytell

Abstract—**The kinematics and hydrodynamics of steady swimming and routine changes in linear swimming velocity were studied in the American eel, *Anguilla rostrata*, using high speed video and particle image velocimetry (PIV). This study presents the first data on how fishes perform small accelerations, which is vital in understanding how to control new biomimetic undulatory propulsors. A detailed analysis of the kinematics of steady swimming from 0.5 to 2 body lengths / second shows that amplitude and frequency are inversely related at a given swimming speed, but average tail velocity and body wave velocity increase linearly with swimming speed. Slip and Strouhal number remain fairly constant at about 0.73 and 0.33, respectively. During steady swimming, the wake consists of strong lateral jets separated by an unstable shear layer. During acceleration, those jets rotate to point downstream to add momentum to the fluid for the eels' accelerations. Wake momentum during acceleration is generally about 2.4 times the necessary inertial force for the eel itself, indicating a strong added mass effect. The thrust, including both the force to overcome fluid dynamic drag and the inertial force, is proportional to a linear combination of kinematic parameters, primarily including average tail velocity, body wave velocity, and tail beat frequency.**

Index Terms— **Acceleration, anguilliform fish swimming, biomimetic propulsors, eels, maneuvering**

I. INTRODUCTION

Fish are highly maneuverable [1;2], sometimes highly efficient [3] swimmers adapted to many diverse environments [4]. Much current submersible research has therefore focused on biomimetics: taking principles of fish swimming and applying them to man-made submersibles (for example, [5-9]). One of the substantial problems in biomimetic vehicles, however, is control, both for simple steady force output and for more complicated actions such as maneuvering and station holding. Traditional propellers, as commonly used on submersibles, are well researched and understood, and thus precise control algorithms can be developed (e.g., [10]). Novel fish-like biomimetic propulsors, including a variety of fin-like appendages [5;6] and fish-like body designs [7;9;11], have both more degrees of freedom than traditional propellers and are less well understood hydrodynamically, making control strategies very difficult to implement. In fact, Barrett [7], in his well-known RoboTuna, were forced to use genetic algorithms simply to find an acceptable combination of parameters to produce steady swimming. Other studies (e.g., [12]) have resorted to computational fluid dynamics to explain describe the force output of a swimming fish. Closed-loop maneuvering seems virtually impossible in the face of such complexity.

Because these artificial propulsors mimic biological systems, the control problem may not be as hard as it seems. Fish swimming provides a baseline for the mechanics and control of artificial undulatory propulsors. Therefore, it is vital to understand the mechanical and hydrodynamic properties of actual biological systems to help design and control artificial systems. Unfortunately, relatively little is known about how fish perform routine maneuvers, such as adjustments in speed, that are required for ordinary tasks like holding station or maintaining speed in turbulent waters. Steady swimming has been studied thoroughly [3;13-15], but only in still water or low-turbulence flow tanks, and extremely rapid accelerations and turns, such as escape responses and feeding strikes, are well known kinematically [2]. This study provides the first data for behaviors between these two extremes: how fish perform routine changes in speed.

Fishes, however, are very diverse, and may not all maneuver in the same way. Different fishes can have extremely different body forms and lifestyles, and are adapted for different behaviors, including high-speed, high-efficiency cruising, rapid turning ability, and high-acceleration impulsive starts. One body design cannot be highly adapted for all of these behaviors simultaneously. Most biomimetic submersible research has focused on high-speed, long-distance swimmers (e.g., [7;9]), such as tunas, marlins, and some sharks. All of these fishes have converged on a similar body plan and particular swimming mode [4], implying that this mode and body shape is advantageous for these behaviors. Recently, submersible research is emphasizing fish maneuvering abilities, which are far beyond those of any man-made vehicle [2;8]. To explain how fishes maneuver, it is

Manuscript submitted July 18, 2003. This work was supported in part by the National Science Foundation under grants IBN9807021 and IBN0316675 to George Lauder.

E. D. Tytell is with Organismic and Evolutionary Biology, Harvard University, Cambridge, MA 02138 USA (phone: 617-496-7199; fax: 617-496-7205; e-mail: tytell@oeb.harvard.edu).

important to examine those that are adapted for maneuvering or swim in a way that makes maneuvering more obvious.

In particular, in this study I examine swimming in the American eel, *Anguilla rostrata*. Eels usually live in complex environments that require substantial maneuvering ability [4]. Other fishes may be more maneuverable, but the swimming kinematics of eels make them suited to this study: they undulate a large portion of their body when they swim, which may make small kinematic changes more obvious than in other fishes. Because virtually no information exists on the mechanics and hydrodynamics of maneuvering in fishes, this study addresses the simplest maneuvering behavior: linear acceleration. This behavior, however, is quite important for ordinary tasks for submersibles. Both holding station and maintaining a constant speed in turbulent water require constant modulation of the propulsor force output, like eels do when they perform small accelerations. It is particularly important to study small accelerations; while high-acceleration fast starts are impressive, they involve major changes in kinematics [2] and are rarely used for routine maneuvering.

I describe steady swimming and then examine how the swimming pattern changes, both kinematically and hydrodynamically, when the eels perform routine changes in speed. From these changes, I build up a picture of how eels change kinematics at different speeds and at different accelerations, and how these kinematic changes affect the wake structure. This helps to define how undulating propulsors, like the eels' bodies and tails, produce force. Ultimately, a detailed description of this force output, given different parameters, such as amplitude, frequency, and overall amplitude envelope, is vital for controlling undulatory propulsors in a stable and predictable way.

A. Review of Fish Swimming

Steady swimming is usually divided into a variety of different modes, based on which fins are used for propulsion and how those fins are used [4]. In particular, one distinction identifies two or three different groups among fishes that use their body and tail fin primarily, and separates them based on how much of the body that undulates. Fishes that undulate a large portion of their bodies are at one end of this spectrum, termed "anguilliform." Most elongate fishes, including eels, many sharks, and needlefish, are anguilliform swimmers. Fishes that undulate less than about a third of their bodies, such as trout, jacks, and bass, are called "carangiform." Often a third category, "thunniform," is added for fish such as tunas and marlins that move their tails fins almost independently from their bodies, although this may just be an extreme form of carangiform swimming [4]. Probably these categories are not actually distinct, but are ends of a continuum. For detailed information on the kinematics of the different modes, see [13;16]. It is important to note, however, that Gray's 1933 study of swimming eels [17], which is often used a description of the anguilliform mode, is now outdated. This study and current research [13] suggest that Gray's eels were swimming in an atypical way, and possibly were accelerating.

The hydrodynamic differences between these steady swimming modes is currently a subject of active research, but it is clear that carangiform swimmers [14;15] produce different wakes than anguilliform swimmers [18]. The wake of a carangiform swimmer resembles a Kármán vortex street in which the signs of the vortices have been reversed, indicating the production of thrust (Fig. 1). In three dimensions, this reverse Kármán street is probably a series of vertical linked vortex rings, inclined to the axis of travel [14]. Less is known about anguilliform swimmers, but, based on data from horizontal planes, this study and [18] indicate that they produce a series of jets perpendicular to the axis of travel, separated by vortices or shear layers (Fig. 1). Müller *et al.* [18] suggest that their planar data correspond to slices through unlinked vortex rings.

Even less is known about the mechanics of maneuvering by fishes. Maneuvering is not only turning, but also acceleration and deceleration. Many studies have assessed how well fishes turn [1;2], but few have examined the details of how fish perform these turns. High-acceleration impulsive starts have been analyzed theoretically [19-21], and several studies have begun to assess the stability of fish swimming and its relationship to maneuverability [22;23]. None of these studies have included experimental hydrodynamic data, and, particularly, no hydrodynamic data exist on linear accelerations, which is vital for understanding how fishes hold station.

II. Methodology

A. Experimental Procedure

American eels (*Anguilla rostrata*) were collected by seine from the Charles River (Cambridge, MA) during June and July 2002 and housed in aquaria at room temperature. Experiments were conducted in a 600 L closed-circuit flow tank with a 26×26×80 cm working section. Animals were confined to the working section using plastic grids with 5×5 cm holes covered in a fine mesh.

Before the experimental procedure, an eel was moved into the flow tank and allowed to acclimate there at a slow swimming velocity for at least an hour. After the acclimation period, eels generally adopted a steady swimming behavior. During the procedure, the animal was gently maneuvered into position in the center of the working section using a wooden probe. Care was taken to remove the probe completely from the region around the eel before data were taken. After a period of steady swimming, most eels would accelerate out of the brightly-lit filming region. Swimming was filmed from below using a digital high-speed camera (RedLake) at 125 or 250 frames/second (fps; Fig. 2).

Kinematic and hydrodynamic data was taken from six individuals, with length L ranging from 12 cm to 24 cm long at swimming speeds from 0.6 L/s to 1.9 L/s and acceleration a from -1.4 L/s^2 to 1.3 L/s^2. From these individuals, 68 swimming sequences consisting of 1280 tail beats in total were analyzed. Of these, 950 beats were during steady

swimming ($|a| < 0.1\ L/s^2$) and 330 were during acceleration.

Particle image velocimetry (PIV; [24]) was used to obtain quantitative flow velocities behind the swimming eel. An approximately 30cm wide horizontal light sheet was projected 7mm above the bottom of the tank using two argon-ion lasers at between 4 and 8 W. The light sheet was filmed using a second digital high-speed camera: either a RedLake camera at 250 fps and 480×420 pixel resolution or a NAC Hi-DCam at 500 fps at 1280×1024 pixel resolution (Fig. 2).

The boundary layer on the bottom of the flow tank was measured to verify that the light sheet was out of the boundary layer. At the lowest flow speeds, the boundary layer was turbulent and approximately 7mm thick; at all speeds, therefore, the light sheet was above the boundary layer.

At each swimming speed, the eel was removed and a mean background flow field was measured. This mean background was subtracted from all flow fields at that speed. Even though the light sheet was out of the boundary layer, turbulent structures such as quasi-streamwise vortices from the bottom would often affect the mean flow. Because these structures often persisted for a long time, their effects could be removed by subtracting this mean background.

B. Data Analysis

Eel outlines and midlines were digitized using a custom Matlab 6.1 (Mathworks) program. After manual identification of an eel's head and tail, the program identified the outline and midline of the eel image using a cross-correlation based technique. Midlines were smoothed simultaneously in both space and time using a smoothing spline to achieve a mean squared error of about 0.25 pix2 (as in [25]). The velocity and acceleration of the body were taken from the point at the tip of the snout. From the midlines, kinematic parameters including the oscillation amplitude at each body point, the oscillation frequency, the tail angle, and the body wave length and speed were calculated. All variables involving a length were normalized by the eel's body length L.

Because the kinematic parameters were all highly correlated with each other and with swimming velocity, a principal components analysis (PCA; [26]) was performed so that kinematic changes could be evaluated in a statistically rigorous way. Two factors explained 69% of the kinematic variation (54% and 15%, respectively). Fig. 3 shows the first factor loadings. The swimming velocity U squared, which is proportional to the drag force [27], was regressed on both components, but only the first component had a significant slope.

Additionally, to evaluate the effects of acceleration separately from those of swimming speed, the maximum and minimum deviation of each kinematic parameter from its median value at a given swimming speed was calculated. These deviations were summed to produce a single reduced value (a principal component score) according to the weights in Fig. 3. The maximum and minimum acceleration at a given speed was regressed on this reduced deviation.

The PIV algorithm was performed using a custom Matlab 6.1 (MathWorks, Inc., Natick, MA) program in two passes using a standard statistical cross-correlation [28] and an error correction technique with an integer pixel estimate of the velocity between passes (as in [29]). Data were smoothed and interpolated onto a regular grid using an adaptive Gaussian window algorithm with the optimal window size (2-3mm for these data; [30]) being careful to note the inherently uneven spacing of PIV data [24].

III. Speed Effects on Steady Swimming

At a particular flow speed, the eels were able to maintain their position with a great deal of fidelity. In the data sets designated as "steady," the maximum acceleration magnitude was less than $0.1\ L/s^2$, and the velocity had a standard error, at most, of about 7%. In most sets, the velocity variation was less than 1%. Animals generally were only able to maintain swimming steadily from about 0.5 L/s to 2 L/s. Below 0.5 L/s, they could hold station on the bottom of the flow tank without swimming, and above 2 L/s, they generally resorted to a burst and coast mode of swimming. The Reynolds numbers for this speed range were between 16 000 and 120 000.

A. Kinematics

All kinematic parameters increased significantly ($P < 0.001$ in all cases) with increasing swimming speed (Fig. 4), although there was substantial variability between individuals. Some parameters showed some non-linearity. In particular, at any given speed, there is an inverse relationship between tail beat amplitude A and frequency f (Fig. 4a,b). Thus, the average tail velocity ($4Af$) is fairly constant at a for specific individuals at a given swimming speed and increases linearly with swimming velocity ($r^2 = 0.771$; Fig. 4c). Body wave velocity V is also almost directly proportional to swimming speed U ($r^2 = 0.882$; Fig. 4d), which meant that the ratio U / V, called "slip" and often used as a measure of efficiency [31], only increased slightly with velocity, and generally remained close to 0.73 (Fig. 4e). Strouhal number, Af / U, was about 0.326 at all swimming speeds, although it varied as much as 0.2 at the slowest swimming speeds. Finally, the body wave length, while tending to increase with swimming speed (Fig. 4f), varied greatly between individuals, with several individuals consistently choosing wave lengths as much as 30% higher than the others. Amplitude always increased exponentially along the body, as $Ae^{\alpha(s-1)}$, where α is an growth parameter and s is the distance along the body (0 at the head to 1 at the tail). Mean r^2 in each data set for the exponential fit was 0.9847±0.0001. The exponential coefficient α decreased from 3.57±0.08 at the lowest swimming speeds to 2.42±0.02 at the highest speeds.

To assess the mechanical differences between kinematics at different swimming speeds, the squared swimming speed U^2, which is proportional to the drag force [27], was regressed on the first principal component PC1 (Fig. 3) of the kinematic variables. Fig. 5 shows the regression. Although there is a lot of scatter, the linear regression between U^2 and PC_1 is highly significant ($P < 0.001$). The regression seems to overestimate

the swimming speed high velocities, indicating that the drag coefficient is probably decreasing at higher speeds.

B. Hydrodynamics

During steady swimming, the wake is dominated by large jets of fluid pointing almost directly laterally, with relatively little downstream flow, unlike the typical carangiform wake [14]. A representative flow field at 1.54 L/s is shown in Fig. 6. These lateral jets are produced along the body in a strong suction region that develops just in front of the tail tip. In particular, when the tail has reached its maximum lateral excursion, and thus has zero velocity, the point just 0.15 L forward of the tail has reached 60.2±0.6% of the swimming velocity. This substantial velocity difference results in a strong suction region that pulls fluid laterally.

Although this wake is similar to that observed by Müller et al. [18], the evolution is somewhat more complex. The tail sheds a single vortex each time it changes direction. As the tail moves towards the other side, it stretches that vortex (A in Fig. 6), producing a shear layer, which breaks down via a Kelvin-Helmholtz instability [27] into two or more vortices. Usually after the breakdown, there is a stronger primary vortex (Fig. 6B) and a weaker secondary vortex (Fig. 6C). This instability is the same at all speeds, although the breakdown proceeds faster at higher speeds. Due to the complexity of the vortex structure, the wake cannot be a simple series of unlinked vortex rings as previously hypothesized [18]. Without an orthogonal plane, however, it is difficult to speculate on the true three-dimensional structure of the wake.

The wake has very little downstream velocity during steady swimming. This is consistent with the balance of forces implied by a constant velocity. However, there is a small downstream increase in momentum, visible at D in Fig. 6: presented as a force coefficient, this is about 0.0017±0.0007 at all swimming speeds. The eel must be pushing fluid out of the way with its head at a rate proportional to $\rho U^2 A_{head}$; as a force coefficient, this is equal to 0.0026 at the tip of the snout. These two values match fairly well, and thus, the net axial momentum added to the fluid is zero.

IV. Acceleration

After a period of steady swimming, all of the eels naturally accelerated out of the filming area due to their dislike of bright lights. Only accelerations that did not involve any substantial turning were analyzed. When the entire eel was visible, the negative accelerations produced as the eels approached the front baffle or a wall were also analyzed. Acceleration varied from -1.4 L/s^2 to 1.3 L/s^2.

A. Kinematics

To separate the effects of acceleration from the effects of swimming at different speeds, in each data set that involved both steady swimming and acceleration, a median value of each kinematic parameter was calculated (the steady state value). The deviation between the parameter's maximum and the steady state value was assumed to be a result of acceleration. Fig. 7 illustrates the change between steady state and the deviation due to acceleration for tail beat amplitude in one swimming sequence.

The most obvious visual effect of acceleration was a large increase in head amplitude (Fig. 8). For example, from steady swimming ($|a| < 0.1$ L/s^2) to accelerating at more than 0.25 L/s^2, the maximum head amplitude increased by 0.0138 L above the steady swimming value, while maximum tail amplitude increased only 0.0045 L above steady state. This results in a general flattening of the amplitude envelope at higher accelerations. In contrast, body wave velocity and wave length remained relatively unaffected by acceleration.

In a similar way as the analysis above for steady swimming, the deviations of all kinematic parameters from their steady swimming values were weighted and summed to produce a principal component score PC1,dev. The maximum acceleration in a given swimming sequence was regressed on this score (Fig. 9), producing a highly significant slope ($P < 0.001$) with an r^2 value of 0.444. Again, the regression underestimates the acceleration magnitude at very high and low accelerations, probably due to changes in added mass [27] as the kinematics change.

B. Hydrodynamics

Fig. 10 shows a representative flow field during an acceleration at 0.6 L/s^2. Before accelerating, this eel was swimming at 1.42 L/s, approximately the same steady speed shown in Fig. 6. Note the reorientation of the jets (Fig. 10A) to point downstream. The primary vortices (Fig. 10B) have increased in strength, but the secondary vortices (Fig. 10C) have not, making them much less distinct. In this set, the 75th percentile of added momentum in the wake was 3.28 mN (as a force coefficient, 0.0052), compared to the maximum force from acceleration of 1.28 mN (force coefficient, 0.0020).

Like above, more momentum is usually present in the wake than is accountable directly to inertial forces due to acceleration (Fig. 11). A regression of maximum inertial force on the 75th percentile of added wake momentum produces a slope of 0.40±0.06, which is significantly different from 1 ($P < 0.001$). The regression was done using maximum acceleration, because acceleration is smoothed by the derivative algorithm, but using only the 75th percentile, not the maximum wake momentum, to minimize the effect of outliers. As was seen above in the kinematic data, the excess wake momentum indicates a substantial effect of added mass. According to these measurements, the average added mass coefficient is thus 1.5±0.4.

V. Discussion

This study is the first to examine the kinematics and hydrodynamics of routine linear accelerations in any fish, and provides the most detail to date on the link between kinematics and hydrodynamics in anguilliform swimmers. This detail is fundamental for the current expanding development of biomimetic undulatory propulsors, because it

provides a baseline for how these propulsors generate force. With this baseline, complex searches for the correct way to undulate, as in [7], become much simpler.

A complication, however, is that there may be many ways to undulate and produce the same force. Anguilliform undulatory locomotion seems to allow substantial freedom in choosing how to produce a force. Most of the eels in this study were of similar size (about 20cm long), but chose to swim in very dissimilar ways. For instance, at a given swimming speed, tail beat frequency and amplitude were observed to vary widely between individuals. However, their ratio stayed fairly constant. During acceleration, however, both undulation frequency and undulation amplitude at all points along the body to accelerate. Other parameters, particularly body wave length, seemed primarily to reflect individual preferences of the eels, with several eels consistently choosing longer body wave lengths than the others, both in absolute length and relative to their body length. Body wave length should decrease during acceleration, because wave velocity tends to remain constant, even as tail beat amplitude and frequency both increase, but this effect was not visible due to the large individual variation. Despite this variability, the swimming kinematics observed in this study are quite consistent with those observed by Gillis [13].

Much like first observed by Müller [18], the anguilliform wakes observed in this study appear quite different from previous observations of the wakes of carangiform swimmers [14;15]. In steady carangiform swimming, there is usually a wavy, downstream fluid jet, meandering between the vortices of the reverse Kármán vortex street (Fig. 1). This has usually been interpreted as evidence for thrust production [14], despite the fact that all data have been collected from steady swimming. Nonetheless, based on the carangiform data, the lack of a "thrust signature" in anguilliform swimming seems somewhat odd. However, even though both cases involved steady swimming, the force distribution on the fishes is different, resulting in a different force balance. Specifically, the bodies of carangiform swimmers tend to have a narrow region between the body and the tail, called the caudal peduncle. The body, which undulates relatively little, produces primarily drag, removing momentum from the fluid. This low momentum fluid concentrates at the caudal peduncle [32]. The tail, like an outboard motor, therefore sees primarily undisturbed flow and produces a thrust wake. Anguilliform swimmers, in contrast, do not usually have a caudal peduncle and undulate a large portion of their bodies; therefore, they produce thrust and drag simultaneously along their bodies. During steady swimming, the two cancel each other out and no downstream momentum is seen in the wake.

Unfortunately, because no thrust is visible in the wake, it is difficult to calculate accurately the efficiency of anguilliform swimming. Generally, anguilliform swimming has been considered to be low efficiency [31], for two reasons: (1) according to inviscid models, all thrust is produced at the tail tip, and therefore body undulation should be minimized for high efficiency, and (2) most large, cruising, predatory fishes, for whom efficient swimming should be very important, have converged on a thunniform swimming mode. However, viscous effects may allow thrust to be generated along the body, and a recent energetic study [33] of eel migration showed them to be almost twice as efficient over the course of a migration as other migratory fishes.

What, therefore, does the observed wake structure indicate about the efficiency? There seems to be substantially more lateral momentum in an eel's wake than in that of a carangiform swimmer, indicating that eels should be less efficient. However, flow was observed to accelerate along the body, indicating the production of thrust anterior to the tail, which may increase their efficiency. Finally, using elongated body theory (EBT; [31]), one can calculate the Froude efficiency η,

$$\eta = 1 - 0.5\,(v_{wave} - U) / v_{wave}. \quad (1)$$

This value ranges from 0.81 at the lowest speeds in this study to 0.89 at the highest. However, EBT consistently underestimates the lateral forces and total power in the wake by as much as twice [34] and thus probably substantially overestimates the efficiency. It will require a more sophisticated modeling approach to resolve this question of the efficiency of anguilliform swimming.

A. Implications for Biomimetic Undulatory Propulsors

Importantly, within the range of velocities and accelerations observed in this study, force is largely linearly proportional to a weighted sum of the kinematic parameters, primarily average tail beat velocity, body wave velocity, and tail beat amplitude. Both the squared velocity, which is proportional to the drag force, and the inertial force were linearly proportional to the first principal component of the kinematic variables with r^2 values of 0.44 or greater. Thus, the total force is also linearly proportional to PC1.

Several recent modeling studies also showed fairly linear force output from oscillatory propulsors. Murray and Howle [35] generated a model that indicated that nonlinear thrust can result from a flapping foil depending on its compliance in heave. For flapping motions in which heave was mostly unrestricted, however, like an untethered fish, thrust was nearly linearly proportional to Strouhal number. Additionally, the simulations in [36] gave evidence for nearly linear thrust production within a Strouhal number range between 0.2 and 0.5, which includes the range normally used by swimming fishes [3].

Therefore, control algorithms for undulatory propulsors may not need to resort to complex strategies like in [7], but rather can choose baseline kinematics from information like that in Fig. 4, and then can vary selected kinematic parameters linearly around the baseline to produce linear changes in force. These propulsors can be very flexible in their choice of which oscillation parameters to modulate, depending on which is most convenient. To reduce noise, for example, it may be important to undulate with a relatively low frequency, but amplitude or wave velocity can be larger to compensate for

the low frequency. Alternatively, to avoid leaving a detectable wake, high frequency and low amplitude undulations may facilitate rapid turbulent wake breakdown; other parameters, such as body wave velocity can compensate. Ultimately, this study provides the first data on how first perform linear accelerations, and also provides a comprehensive kinematic and hydrodynamic baseline for how anguilliform fishes swim. With this baseline, future generations of biomimetic undulatory propulsors can be better designed and controlled for steady motion and maneuvering in turbulent water.

FIGURE CAPTIONS

Fig. 1—Schematic of the swimming mode and wakes of (a) carangiform and (b) anguilliform swimmers. Midlines (heavy line) and approximate amplitude envelopes (thin lines) are shown for both modes. Carangiform midline provided by J. Liao.

Fig. 2—Experimental filming and PIV configuration. Representative images from each camera are shown to the left.

Fig. 3—Factor loading for the first principal component PC_1 in the principal component analysis. The whole bar is scaled to represent the total variance explained by PC_1 and the sections are scaled to represent the contribution of each variable. Numerical loadings are shown above and below the bar. v_{tail}, average tail velocity; v_{wave}, body wave velocity; $A_{50\%}$, fractional amplitude relative to the tail at the body midpoint; A, tail amplitude; $A_{95\%}$, fractional amplitude relative to the tail at 95% of the body length; f, tail beat frequency; A_{head}, fractional amplitude relative to the tail at the head; θ_{tail}, maximum angle of the tail to the swimming direction; λ, body wave length; $\Delta\phi_{tail}$, phase lag between the maximum tail angle and the maximum lateral excursion of the tail.

Fig. 4—Swimming kinematics at a range of swimming speeds. The boxes at each data point range from the first to third quartile with a line at the median, whiskers are 1.5 times the inter-quartile range long, and any outliers are plotted as dots. Notches show approximate 95% confidence intervals. All plots have the same x axis scale. Regression lines are shown in black, and all regressions are highly significant ($P < 0.001$). Different fills and shades of gray indicate different individuals. Dotted lines in (c) and (d) indicate a one-to-one relationship.

Fig. 5—Swimming velocity squared plotted against the first principal component PC_1 of the kinematic variables (defined in Fig. 3). A highly significant ($P < 0.001$) regression line is shown as a thick line with a 95% confidence interval around the line shown in gray. The r^2 value and regression equation are shown at the bottom of the plot.

Fig. 6—Representative wake flow field from a 22 cm long eel swimming at 1.54 L/s. This field is an average of 14 fields at the same tail beat phase. Vector lengths are proportional to the magnitude of the flow at that point. For velocities less than 2.5 cm/s, arrowheads remain visible to indicate velocity direction. Vorticity is shown in gray and white in the background, with the sign indicated by the direction of the arrows. The tip of the eel's tail is visible on the left in black. Important flow regions are indicated by letters and explained in the text.

Fig. 7—Representative change in tail beat amplitude (filled circles) during an acceleration (solid line) from steady swimming at 1.53 L/s, showing the definitions of the steady state value for a kinematic parameter, and its deviation due to acceleration. Steady swimming is at times earlier than 2.8 s (vertical dotted line), and the steady state value for amplitude is shown by the horizontal dotted line. The deviation, shown by the solid arrow, is the difference between the maximum amplitude and the steady state value.

Fig. 8—Undulation amplitude envelopes at each body point for different accelerations from steady swimming at about 1.5 L/s. Standard error around each of the accelerational envelopes is indicated by a gray region. The envelope for steady swimming is shown with a thick black line.

Fig. 9—Acceleration plotted against the kinematic deviation principal component (see text for explanation). A highly significant regression line ($P < 0.001$) is indicated with a thick line and a 95% confidence interval around the regression is shown in gray. The regression equation and r^2 value are shown at the bottom of the plot.

Fig. 10—Representative wake flow field from a 24 cm long eel accelerating at 0.6 L/s^2, starting from steady swimming at 1.42 L/s. This field is an average of 3 fields at the same tail beat phase during the acceleration. Vector lengths are proportional to the magnitude of the flow at that point. For velocities less than 2.5 cm/s, arrowheads remain visible to indicate velocity direction. Vorticity is shown in gray and white in the background, with the sign indicated by the direction of the arrows. Note the different vorticity scale from Fig. 6. The tip of the eel's tail is out of view on the left. Important flow regions are indicated by letters and explained in the text.

Fig. 11—Inertial force due to acceleration plotted against added wake momentum flux. The highly significant ($P < 0.001$) regression line is indicated by a solid thick line with a 95% confidence interval around the line shown in gray. The r^2 value and regression equation are shown at the bottom of the plot. A one-to-one relationship is indicated by the thin dotted line. m, eel's mass; ρ, fluid density; U, mean flow speed; A, area affected by the eel, equal to the width of the wake multiplied by the measured height of the eel; u, velocity fluctuations around U.

REFERENCES

[1] Webb, P. W., "Speed, acceleration and manoeuvrability of two teleost fishes," *J.Exp.Biol.*, vol. 102, pp. 115-122, 1983.

[2] Domenici, P. and Blake, R. W., "The kinematics and performance of fish fast-start swimming," *J.Exp.Biol.*, vol. 200, pp. 1165-1178, 1997.

[3] Triantafyllou, M. S., Triantafyllou, G. S., and Yue, D. K. P., "Hydrodynamics of fishlike swimming," *Ann.Rev.Fluid Mech.*, vol. 32, pp. 33-53, 2000.

[4] Helfman, G. S., Collette, B. B., and Facey, D. E., *The Diversity of Fishes*, London: Blackwell Science, 1997.

[5] Kemp, M., Hobson, B., Janét, J., Pell, C. A., and Tytell, E. D., "Assessing the performance of oscillating fin thruster vehicles," in 12th *Int.Symp.Unmanned Untethered Submersible Tech*, Lee, NH, 2001.

[6] Kato, N., "Control performance in the horizontal plane of a fish robot with mechanical pectoral fins," *IEEE J.Oceanic Eng.*, vol. 25, no. 1, pp. 121-129, 2000.

[7] Barrett, D., "Propulsive efficiency of a flexible hull underwater vehicle." Ph.D. Dissertation, Department of Ocean Engineering, Massachusetts Institute of Technology, 1996.

[8] Bandyopadhyay, P. R., "Maneuvering hydrodynamics of fish and small underwater vehicles," *Integ.Comp.Biol.*, vol. 42, pp. 102-117, 2002.

[9] Anderson, J. M. and Kerrebrock, P. A., "The vorticity control unmanned undersea vehicle (VCUUV) performance results," in 11th *Int.Symp.Unmanned Untethered Submersible Tech.*, Lee, NH, 1999, pp. 360-369.

[10] Whitcomb, L. and Yoerger, D. R., "Development, comparison, and preliminary experimental validation of nonlinear dynamic thruster models," *IEEE J.Oceanic Eng.*, vol. 24, no. 4, pp. 481-494, 1999.

[11] Ayers, J., Wilbur, C., and Olcott, C., "Lamprey robots," in *Proc.Int.Symp.Aqua Biomechanisms*, Tokai, Japan, 2000.

[12] Wolfgang, M. J., Anderson, J. M., Grosenbaugh, M. A., Yue, D. K. P., and Triantafyllou, M. S., "Near-body flow dynamics in swimming fish," *J.Exp.Biol.*, vol. 202, pp. 2303-2327, 1999.

[13] Gillis, G. B., "Undulatory locomotion in elongate aquatic vertebrates: Anguilliform swimming since Sir James Gray," *Amer.Zool.*, vol. 36, no. 6, pp. 656-665, 1996.

[14] Lauder, G. V., "Function of the caudal fin during locomotion in fishes: Kinematics, flow visualization, and evolutionary patterns," *Amer.Zool.*, vol. 40, no. 1, pp. 101-122, 2000.

[15] Müller, U. K., van den Heuvel, B.-L. E., Stamhuis, E. J., and Videler, J. J., "Fish foot prints: Morphology and energetics of the wake behind a continuously swimming mullet (*Chelon labrosus* risso)," *J.Exp.Biol.*, vol. 200, pp. 2893-2906, 1997.

[16] Sfakiotakis, M., Lane, D. M., and Davies, J. B. C., "Review of fish swimming modes for aquatic locomotion," *IEEE J.Oceanic Eng.*, vol. 24, no. 2, pp. 237-252, 1999.

[17] Gray, J., "Studies in animal locomotion. I. The movement of fish with special reference to the eel," *J.Exp.Biol.*, vol. 10, pp. 88-104, 1933.

[18] Müller, U. K., Smit, J., Stamhuis, E. J., and Videler, J. J., "How the body contributes to the wake in undulatory fish swimming: flow fields of a swimming eel (*Anguilla anguilla*)," *J.Exp.Biol.*, vol. 204, no. 16, pp. 2751-2762, 2001.

[19] Weihs, D., "A hydrodynamical analysis of fish turning manoevers," *Proc.R.Soc.Lond.B*, vol. 182, pp. 59-72, 1972.

[20] Weihs, D., "The mechanism of rapid starting of slender fish," *Biorheology*, vol. 10, pp. 343-350, 1973.

[21] Wakeling, J. M. and Johnston, I. A., "Body bending during fast-starts in fish can be explained in terms of muscle torque and hydrodynamic resistance," *J.Exp.Biol.*, vol. 202, no. 6, pp. 675-682, 1999.

[22] Webb, P. W., "Control of posture, depth, and swimming trajectories of fishes," *Integ.Comp.Biol.*, vol. 42, pp. 94-101, 2002.

[23] Weihs, D., "Stability *versus* maneuverability in aquatic locomotion," *Integ.Comp.Biol.*, vol. 42, pp. 127-134, 2002.

[24] Willert, C. E. and Gharib, M., "Digital particle image velocimetry," *Exp.Fluids*, vol. 10, no. 4, pp. 181-193, 1991.

[25] Walker, J. A., "Estimating velocities and accelerations of animal locomotion: A simulation experiment comparing numerical differentiation algorithms," *J.Exp.Biol.*, vol. 201, pp. 981-995, 1998.

[26] Jackson, J. E., *A User's Guide to Principal Components*, New York: John Wiley and Sons, 1991.

[27] Faber, T. E., *Fluid Dynamics for Physicists*, Cambridge: Cambridge University Press, 1995.

[28] Fincham, A. M. and Spedding, G. R., "Low cost, high resolution DPIV for measurement of turbulent fluid flow," *Exp.Fluids*, vol. 23, pp. 449-462, 1997.

[29] Hart, D. P., "Super-resolution PIV by recursive local-correlation," *J.Visual.*, vol. 10, pp. 1-10, 1999.

[30] Agüí, J. C. and Jiménez, J., "On the performance of particle tracking," *J.Fluid Mech.*, vol. 185, pp. 447-468, 1987.

[31] Lighthill, M. J., "Aquatic animal propulsion of high hydromechanical efficiency," *J.Fluid Mech.*, vol. 44, pp. 265-301, 1970.

[32] Nauen, J. C. and Lauder, G. V., "Locomotion in scombrid fishes: Morphology and kinematics of the finlets of the chub mackerel *Scomber japonicus*," *J.Exp.Biol.*, vol. 203, pp. 2247-2259, 2000.

[33] van Ginneken, V. J. T., Antonissen, E., and van den Thillart, G. E. E. J. M., "The 6000-km migration run of European eel: Remarkably low energy costs," presented at American Physiological Society Annual Meeting, San Diego, 2002.

[34] Tytell, E. D. and Lauder, G. V., "Balancing thrust and drag: The hydrodynamics of anguilliform locomotion in steadily swimming eels (*Anguilla rostrata*)," *Comp.Biochem.Physiol.*, vol. 134, no. 3 (Supplement), p. S53, 2003.

[35] Murray, M. and Howle, L. E., "Spring stiffness influence on an oscillating propulsor," *J.Fluids Struct.*, vol. 17, pp. 915-926, 2003.

[36] Pedro, G., Suleman, A., and Djilali, N., "A numerical study of the propulsive efficiency of a flapping hydrofoil," *Int.J.Num.Meth.Fluids*, vol. 42, no. 5, pp. 493-526, 2003.

Figure 1

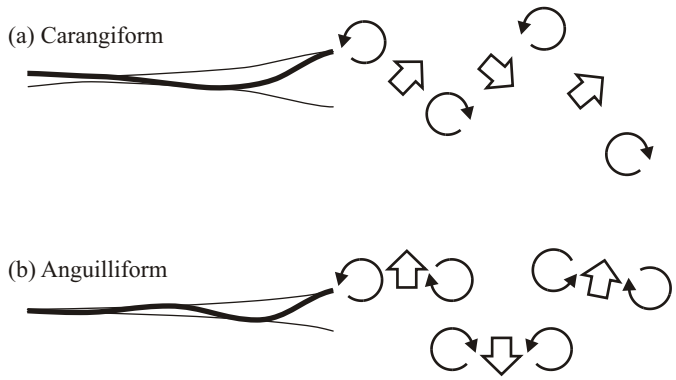

Figure 2

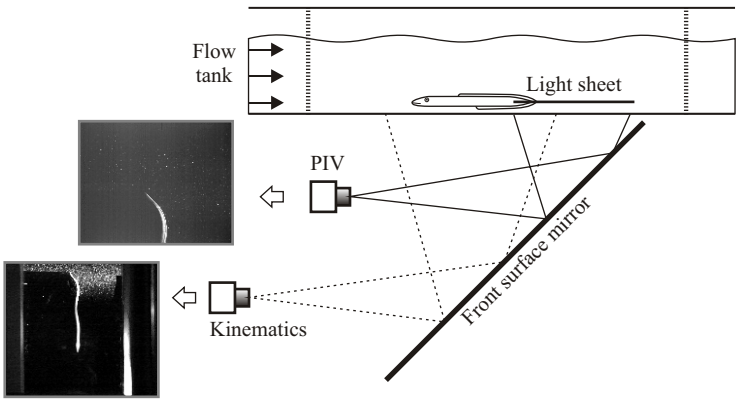

Figure 3

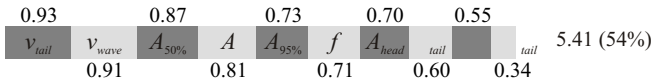
0.93
0.87
0.73
0.70
0.55
v_{tail}
v_{wave}
$A_{50\%}$
A
$A_{95\%}$
f
A_{head}
$_{tail}$
$_{tail}$
0.91
0.81
0.71
0.60
0.34
5.41 (54%)

Figure 4

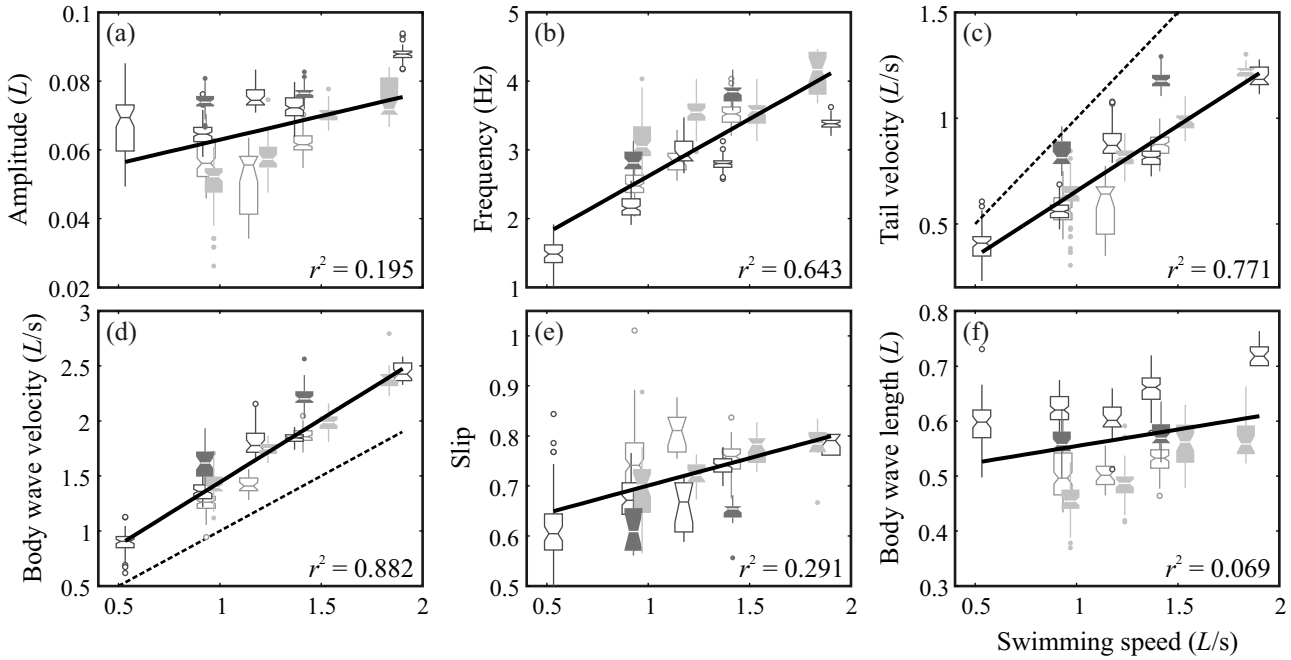
(a)
Amplitude (L)
r^2 = 0.195
(b)
Frequency (Hz)
r^2 = 0.643
(c)
Tail velocity (L/s)
r^2 = 0.771
(d)
Body wave velocity (L/s)
r^2 = 0.882
(e)
Slip
r^2 = 0.291
(f)
Body wave length (L)
r^2 = 0.069
Swimming speed (L/s)

Figure 5

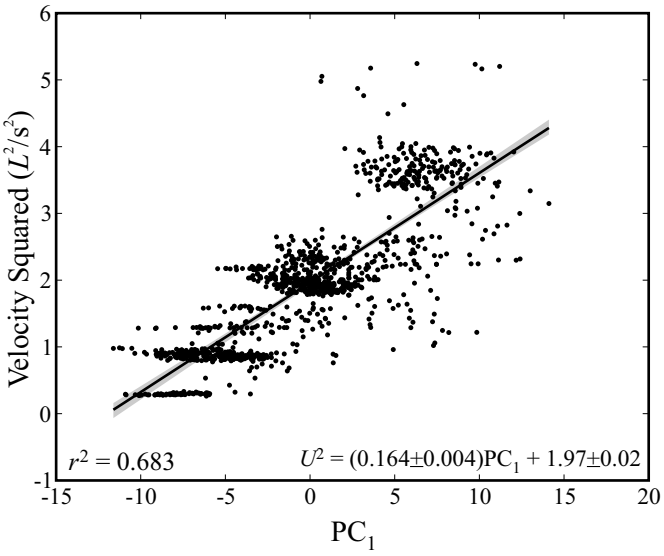
Velocity Squared (L^2/s^2)
PC_1
$r^2 = 0.683$
$U^2 = (0.164\pm0.004)PC_1 + 1.97\pm0.02$
6
5
4
3
2
1
0
-1
-15
-10
-5
0
5
10
15
20

Figure 6

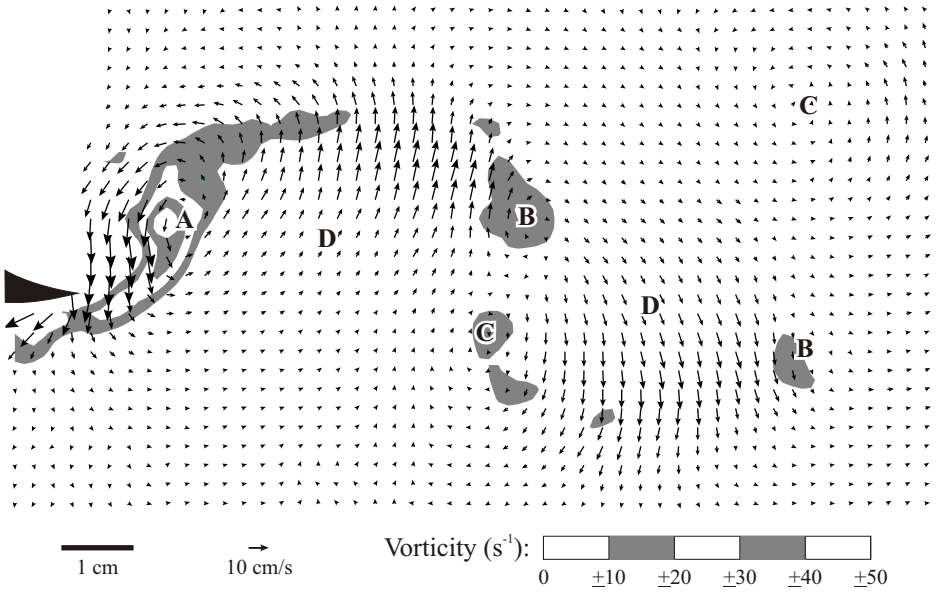

Figure 7

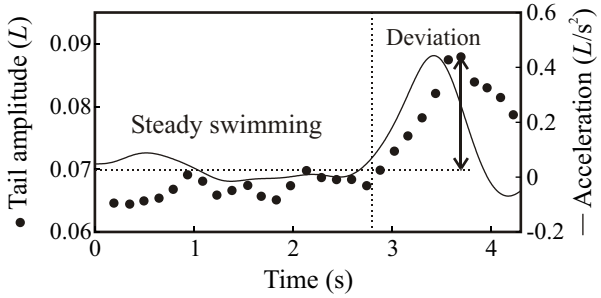
Deviation
Steady swimming
Tail amplitude (L)
Acceleration (L/s²)
Time (s)
0.09
0.08
0.07
0.06
0.6
0.4
0.2
0
-0.2
0
1
2
3
4

Figure 8

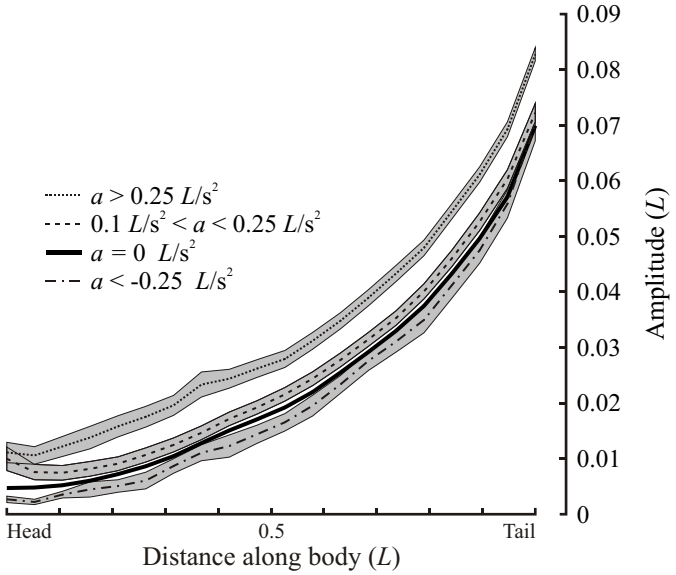
$a > 0.25\ L/s^2$
$0.1\ L/s^2 < a < 0.25\ L/s^2$
$a = 0\ L/s^2$
$a < -0.25\ L/s^2$
0.09
0.08
0.07
0.06
0.05
0.04
0.03
0.02
0.01
0
Amplitude (L)
Head
0.5
Tail
Distance along body (L)

Figure 9

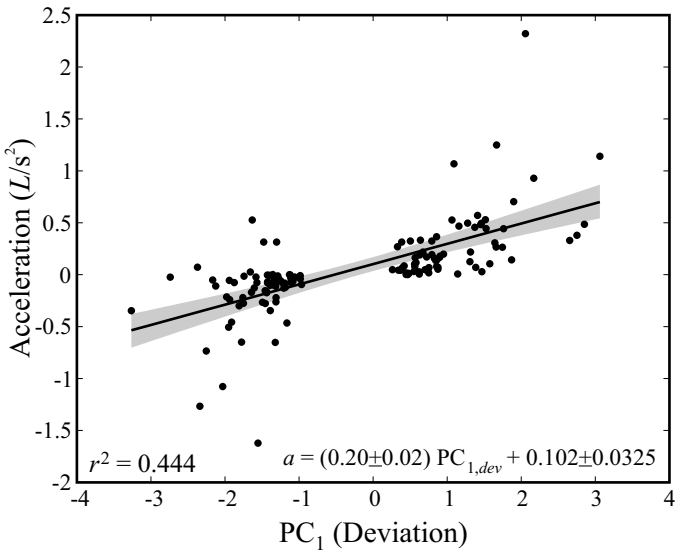
2.5
2
1.5
1
0.5
0
-0.5
-1
-1.5
-2
-4
-3
-2
-1
0
1
2
3
4
Acceleration (L/s^2)
PC_1 (Deviation)
$r^2 = 0.444$
$a = (0.20\pm0.02)\ PC_{1,dev} + 0.102\pm0.0325$

Figure 10

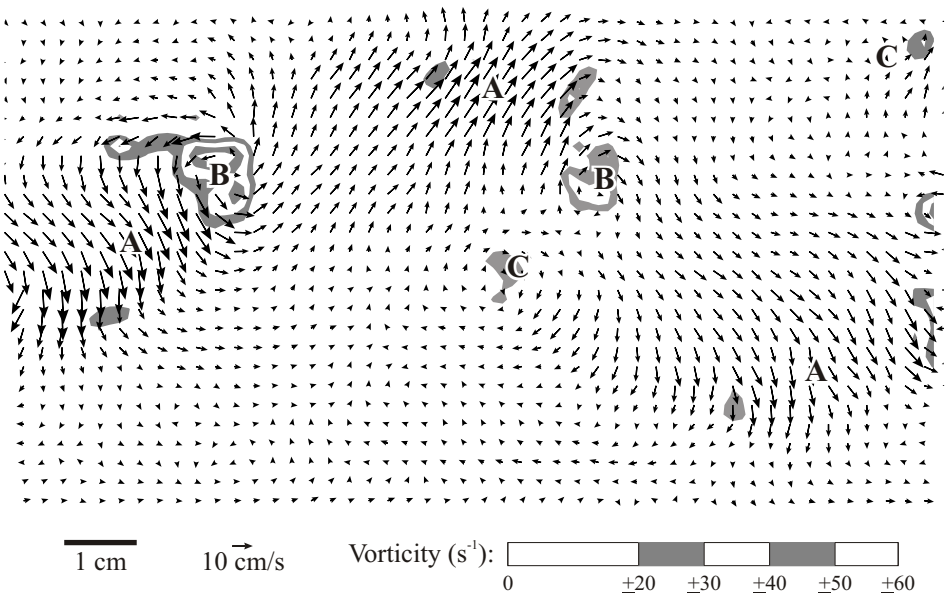

Figure 11

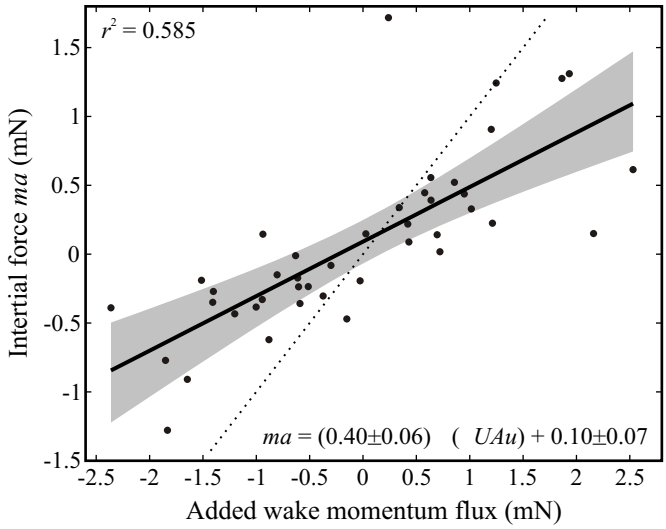
r^2 = 0.585
ma = (0.40±0.06) (UAu) + 0.10±0.07
Intertial force ma (mN)
Added wake momentum flux (mN)
1.5
1
0.5
0
-0.5
-1
-1.5
-2.5
-2
-1.5
-1
-0.5
0
0.5
1
1.5
2
2.5